Am J Transl Res 2018;10(5):1469-1480
www.ajtr.org /ISSN:1943-8141/AJTR0071470

Original Article

Application of real-time three-dimensional contrast-enhanced ultrasound using SonoVue for the evaluation of focal liver lesions: a prospective single-center study

Ying Lu[1*], Baoxian Liu[1*], Yanling Zheng[1], Jia Luo[1], Xiaoer Zhang[1], Guangliang Huang[1], Xiaohua Xie[1], Jieyi Ye[1], Wei Wang[1], Xusheng Liu[2], Xiaoyan Xie[1]

[1]Department of Medical Ultrasound, Institute of Diagnostic and Interventional Ultrasound, The First Affiliated Hospital of Sun Yat-sen University, Guangzhou Guangdong Province, P. R. China; [2]Department of Burns, The First Affiliated Hospital of Sun Yat-sen University, Guangzhou, China. [*]Equal contributors.

Received December 24, 2017; Accepted April 6, 2018; Epub May 15, 2018; Published May 30, 2018

Abstract: Focal liver lesions (FLLs) include a variety of benign and malignant tumors, and are usually differential diagnosed by ultrasonography. However, traditional two-dimensional contrast-enhanced ultrasound (2D-CEUS) can evaluate a single slice of a lesion. It cannot fully display perfusion of a lesion and the relationship with the surrounding tissues, which may lead to misdiagnosis. This study aimed to investigate real-time three-dimensional CEUS (3D-CEUS) for evaluation of the vascular configuration of FLLs. Using real-time 3D-CEUS with SonoVue on 161 patients with FLLs, we found that when compared with 2D-CEUS, real-time 3D-CEUS provided more detailed information about the origin, continuity, and numbers and structures of the feeding artery. On 3D-CEUS hepatocellular carcinoma showed intratumoral vessels with diffuse enhancement, metastatic liver cancer showed peritumoral vessels or absence of tumor vessels with ring-like enhancement or non-enhancement, focal nodular hyperplasia showed a spoke-wheel artery with diffuse enhancement, and hemangiomas showed nodular enhancement. Our results demonstrate that real-time 3D-CEUS using SonoVue is an effective method for visualizing the characteristic vascular configuration of FLLs, and this may assist with the diagnosis.

Keywords: Real-time three-dimensional contrast-enhanced ultrasound, focal liver lesions, vascular configuration

Introduction

Focal liver lesions (FLLs) include a variety of benign and malignant tumors, such as hepatocellular carcinoma (HCC), metastatic liver cancer (MLC), hemangiomas, focal nodular hyperplasia (FNH), and inflammatory lesions. Ultrasonography has emerged as an excellent tool for the differential diagnosis of FLLs.

Recently, with the help of low acoustic power contrast-specific modes with a mechanical index of less than 0.2, and second-generation contrast agents such as SonoVue, two-dimensional contrast-enhanced ultrasound (2D-CEUS) has been widely used for distinguishing malignant from benign FLLs [1-3]. However, 2D-CEUS can only evaluate a single slice of a lesion, and cannot fully display a lesions perfusion and relationship with the surrounding tissues. Because of this, using 2D-CEUS may lead to a misdiagnosis. Previous studies have suggested that three-dimensional CEUS (3D-CEUS) possesses advantages over 2D-CEUS as it can display the spatial relation of a lesion with surrounding tissues [4, 5]. With 3D-CEUS the volume data can be rotated to different angles to establish the best position of an image to fully analyze a selected region. This ability compensates for the single-plane limitation of 2D-CEUS. However, conventional 3D-CEUS provides a static image, and does not provide enhancement patterns along with an evolving phase [6].

Real-time 3D-CEUS with continuous data set acquisition capacity is called 4D-CEUS. The technique can accurately illustrate the location

of a lesion, indicate the spatial relation of liver tumor blood vessels, and visualize the dynamic perfusion of 3D regions of interest to provide richer and more intuitive information [7]. As such, it has advantages for displaying angiographic structure and dynamic perfusion of FLLs in real-time.

The aim of the current study was to demonstrate morphological images of feeding arteries and spatial tumor enhancement patterns of FLLs on the real-time 3D-CEUS images, and to investigate the effectiveness of real-time 3D-CEUS in the differentiation of FLLs.

Materials and methods

This prospective study was approved by the Institutional Ethics Committee of the First Affiliated Hospital of Sun Yat-sen University (Guangzhou, People's Republic of China), and informed consent was obtained.

Patients

Between June 2013 and April 2014, patients suspected of having FLLs by prior conventional US or computed tomography (CT) were recruited to undergo real-time 3D-CEUS. For patients with multiple lesions, real-time 3D-CEUS was performed on the largest lesion, and if the largest lesion was not suitable for scanning due to its location, the next largest lesion was selected.

The eligibility criteria for participation in the study were: a) age 18-80 years, b) absence of severe cardiopulmonary diseases, c) absence of pregnancy or lactation, d) pathologically or clinically diagnosed FLLS, and e) untreated FLLs. The reference standards for FLLs in this study were as previously described [8]. HCC was diagnosed based upon pathological examination of ultrasound-guided biopsy or surgical resection specimen, or according to the diagnostic criteria published by the European Association for the Study of the Liver (EASL). MLC was diagnosed by ultrasound-guided biopsy, or based clinical data (history of malignant tumor and the new liver lesions with typical imaging finding, i.e., arterial-phase hyperenhancement and quick contrast washout on images). Benign tumors were confirmed by their typical appearance on multi-detector contrast-enhanced CT, or magnetic resonance imaging (MRI) with at least 6-months of follow-up, and those without typical findings were confirmed by pathological examination.

Patients who were unable to hold their breath, or had lesions in inappropriate locations for acquiring 3D images due to artifacts from costal bone shadows, heart motion, or abdominal gas were excluded.

CEUS examination

The same sonographer (XYX) with more than 15 years of experience performing abdominal US and more than 10 years of experience performing CEUS and 3D-CEUS performed all the examinations using a Toshiba Aplio 500 US imaging system (Toshiba Medical Systems, Tokyo, Japan). A convex transducer (PVT-375BT) with a center frequency of 3.5 MHz was used for 2D scanning, and a 4D transducer (PVT-675MVT) with a frequency range of 4-8 MHz was used for real-time 3D-CEUS.

Before the administration of the contrast agents, baseline grayscale ultrasound scans of the entire liver were performed. The imaging settings of the ultrasound scanner were optimized to get the best depiction of the target lesion, and the details of the lesions were recorded. Color Doppler flow imaging (CDFI), or advanced dynamic flow imaging (ADFI) was also performed to assess the blood flow.

2D-CEUS was then performed using contrast harmonic imaging. A bolus of 2.4 mL of ultrasound contrast agent (SonoVue, Barcco, Milan, Italy) was injected intravenously in an antecubital vein, followed by a flush of 5 mL of normal saline. Continuous scanning began immediately after SonoVue administration, and continued for 3-5 min. The imaging process was continuously monitored, and classified into arterial phase (i.e., 7-30 s after contrast agent injection), portal phase (31-120 s), and late phase (121-360 s) [9]. Digital cine clips were recorded and stored for subsequent analysis. The field of view and gain was optimized to provide the clearest depiction of the lesion. A split-screen mode was used to display the CEUS image on the right side, and the background US image on the left side on a single monitor.

Subsequently, at an interval of at least 5 min to allow for contrast clearance of the previous contrast injection, real-time 3D-CEUS was performed. A second dose of 2.4 mL of SonoVue

was administered without saline flush, and the equipment settings and parameters were the same as used for 2D-CEUS. The real-time 3D-CEUS scanning was initiated when the liver artery was visualized. The transducer was kept stable to ensure that the target lesion was in the scan area during the arterial and early portal phases, and the raw data clips were stored for subsequent image reconstruction and analysis.

3D image reconstruction

One author (YL with 5 years of experience in abdominal US, CEUS, and 3D-CEUS), who was blinded to the clinical information, final diagnosis, and other radiological findings, reconstructed the 3D images using the Aplio 500 online analysis software package (CHI-Q, Version 3.7, Toshiba, Japan). The reformatted images of the three orthogonal planes were displayed instantaneously on the screen. The images were rotated or translated to obtain the optimal viewing orientation, and the size of the subvolume was adjusted to eliminate unwanted echoes. Various 3D modes were available with the scanner, including a tomographic ultrasound imaging (TUI) mode. The TUI mode could display the target lesion in a series of parallel planes, with a thinnest interval distance of 0.2 mm, along the A, B, or C plane. These images in optimal mode were also displayed dynamically to ensure better observation from various directions, and better understanding of the spatial relation between the target lesion and adjacent structures. The whole process of reconstruction took 3-5 min for each patient. Technical success was defined as the successful reconstruction of real-time 3D-CEUS images. The 3D-CEUS data sets were stored digitally, and transferred to a high-performance personal computer for subsequent analysis.

3D images analysis

Two investigators (GLH and XHX, both with more than 8 years experience in US, CEUS, and 3D-CEUS) evaluated the images, and differences were resolved by consensus. Both investigators were blinded to the final diagnoses, clinical information, and other radiological findings.

For real-time 3D-CEUS images, the imaging quality, feeding arteries, and tumor enhancement patterns in the early phase for all the lesions were reviewed. The assessment of the imaging quality of real-time 3D-CEUS was classified into four grades: *excellent, good, common* and *poor. Excellent* indicated that the lesion and feeding arteries were clearly displayed without artifact, the continuity of vessels was clear, and the whole image was uniform. *Good* indicated that the lesion and feeding arteries were displayed with little artifact, and the whole image was uniform. *Common* indicated that the lesion and feeding arteries were depicted with significant artifact, or the image was not uniform. *Poor* indicated that the lesion and feeding arteries were not clearly visualized, and the image could not be further assessed. The potential influence of the pathological diagnosis, lesion size, location, scanning approach, presence of interfering shadowing, and enhancement level on 3D-CEUS image quality was investigated. An interference shadow was defined as acoustic shadowing from the ribs, and gas from the stomach, intestine, or colon. Real-time 3D-CEUS was also compared with 2D-CEUS in assessing the origin (clear or unclear) and continuity (well or poor) of the feeding arteries. The number of feeding arteries and structure (tortuous or normal) were further compared in subgroups of each histological lesion type.

Lesions with acceptable image quality (including excellent, good, and common) were further evaluated for tumor enhancement patterns. The tumor enhancement patterns consisted of tumor vessels and tumor enhancements, which were divided in four types and four patterns, respectively.

The four types of tumor vessels were defined as follows: *intratumoral vessels*, tortuous vessels distributed in the lesions; *spoke-wheel artery*, a centrally located feeding artery with centrifugal satellite branching; *peritumoral vessels*, tumor vessels mainly distributed at the periphery of the lesions; and *absence of tumor vessels*. The intratumoral vessels were classified according to three patterns: surrounding pattern, branching pattern, and mixed artery pattern. The surrounding pattern was defined as the nourishing artery distributed from the periphery to the center of the lesion; branching pattern was defined as the nourishing artery located in the center of the lesion, with branches distributed to the periphery of the lesion. The four patterns of tumor enhance-

Table 1. Image quality of real-time 3D-CEUS for characterization during arterial phase and the potential influence factors

Influencing factors	Image quality				*P* value
	Excellent (n = 90)	Good (n = 18)	Common (n = 24)	Poor (n = 29)	
Pathology					
Malignant (n = 132)	74	11	20	27	0.051
Benign (n = 29)	16	7	4	2	
Lesion size					
≤ 3.0 cm (n = 44)	22	5	6	11	0.555
> 3.0 cm (n = 117)	68	13	18	18	
Lesion location					
Left lobe (n = 36)	15	5	7	9	0.274
Right lobe (n = 125)	75	13	17	20	
Depth scanning route					
Intercostal (n = 107)	66	14	9	18	0.007
Subcostal (n = 54)	24	4	15	11	
Presence of interfering shadowing					
Yes (n = 37)	3	11	10	13	< 0.001
No (n = 124)	87	7	14	16	
Intralesional enhancement level in arterial phase					
Hyperenhancement (n = 129)	87	16	16	10	< 0.001
Isoenhancement (n = 6)	0	1	0	5	
Hypo-or non-enhancement (n = 26)	3	1	8	14	

ments included *diffuse enhancement*, defined as homogeneous or heterogeneous tumor enhancement; *peripheral ring-like enhancement,* defined as ring-shaped enhancement in the tumor periphery; *peripheral nodular enhancement*, defined as enhancement in the tumor periphery with a nodular shape; and *absence of tumor enhancement* compared with the adjacent liver parenchyma.

Statistical analysis

Quantitative variables were expressed as the mean ± standard deviation. Categorical variables were expressed as relative frequency. Factors potentially influencing image quality, such as lesion size, lesion location, lesion depth, scanning approach, interfering factors, and intralesion enhancement level in the arterial phase, were evaluated using chi-square tests. Categorical variables measured on real-time 3D-CEUS and 2D-CEUS images were also compared using chi-square tests, and the sensitivity, specificity, positive predictive value, negative predictive value, and accuracy were calculated. All statistical analyses were performed using SPSS version 16.0 (SPSS, Chicago, IL). A two-tailed *P* value < 0.05 was considered significant.

Results

A total of 161 patients were enrolled in the study. There were 125 males and 36 females, with a mean age of 49.6 ± 14.0 years (range, 32-71 years). Among them, 103 patients had solitary tumors, and 58 had multiple tumors. For patients with multiple lesions, only the largest one was selected for evaluation. Thus, 161 lesions with a mean diameter of 5.5 ± 3.2 cm (range, 1.3-11.7 cm) were examined. There were 132 malignant lesions, and 29 benign lesions. Among the malignant lesions, 109 were HCC (39 diagnosed by clinical criteria, 70 confirmed by pathological examination), 3 were intrahepatic cholangiocarcinoma (ICC), and 20 were MLC (all diagnosed based upon clinical data) from colon carcinoma (n = 7), rectal carcinoma (n = 5), gastrointestinal stromal tumor (n = 1), pancreatic neuroendocrine tumor (n = 1), pancreatic carcinoma (n = 1), esophageal carcinoma (n = 1), ampullary carcinoma (n = 1), and breast cancer (n = 5). The 29 benign tumors consisted of 16 hemangiomas and 13 FNHs.

Table 2. The origin and continuity of feeding arteries on real-time 3D-CEUS and 2D-CEUS images (n = 161)

	Origin		Continuous arrangement	
	Clear	Unclear	Well	Poor
2D-CEUS	90	71	77	84
Real-time 3D-CEUS	109	52	110	51

Table 3. The feeding artery numbers on real-time 3D-CEUS and 2D-CEUS images (n = 161)

	Feeding artery numbers					*P* value
	1	2	3	> 3	0/unclear	
Malignant lesions (n = 132)						
2D-CEUS	51	15	8	6	52	0.005
Real-time 3D-CEUS	36	29	19	10	38	
Benign lesions (n = 29)						
2D-CEUS	7	1	0	0	21	0.387
Real-time 3D-CEUS	11	2	0	0	16	

Table 4. The feeding artery structures on real-time 3D-CEUS and 2D-CEUS images (n = 109)

	Feeding artery structures			*P* value
	Tortuous	Normal	Unclear	
Malignant lesions				
2D-CEUS	47	17	59	0.017
Real-time 3D-CEUS	69	10	44	
Benign lesions				
2D-CEUS	2	1	26	0.458
Real-time 3D-CEUS	1	6	22	

Three hemangiomas and 4 FNHs with atypical radiologic findings were confirmed with biopsy, and the remaining 22 lesions were diagnosed by CT/MRI with the clinical data.

Influencing factors for the image quality of real-time 3D-CEUS

The technical success was 100% (161/161). During the arterial phase, the image quality of the 161 lesions was determined to be "Excellent" in 82 (54.3%) lesions, "Good" in 17 (11.3%) lesions, "Common" in 23 (15.2%) lesions, and "Poor" in 29 (19.2%) lesions. After review of the real-time 3D-CEUS images, interfering shadowing was present in 37 (23.0%) of 161 lesions. Intercostal scanning was performed in 107 (66.5%) patients, and the remaining 54 (33.5%) patients were scanned from a subcostal approach. Hyper-, iso-, and hypo- or non-enhancement was visualized in 129 (80.1%), 6 (3.7%), and 26 (16.1%) lesions, respectively. "Excellent" image quality was found in 67.4% (87/129) hyperenhanced lesions and in 11.5% (3/26) hypo- or non-enhanced lesions. No isoenhanced lesions were scored as having "Excellent" image quality.

Among the potential influencing factors, the scanning approach, presence of interfering shadowing, and intralesional enhancement extent in the arterial phase correlated with the image quality of real-time 3D-CEUS. The lesion location, size and depth did not have a significant influence on the image quality (**Table 1**).

Among the 29 lesions with poor imaging quality, there were 27 malignant tumors (3 ICCs, 17 HCCs and 7 MLCs) and 2 benign tumors (2 hemangiomas). Comparison of the lesions with acceptable imaging quality and poor imaging quality showed significant differences in interfering shadowing ($P = 0.002$) and enhancement level in the arterial phase ($P < 0.001$).

Real-time 3D-CEUS versus 2D-CEUS in the evaluation of the feeding artery

The comparison of real-time 3D-CEUS and 2D-CEUS showed significant differences in both the origin ($P = 0.029$) and continuity ($P < 0.001$) of the feeding artery (**Table 2**).

In the subgroup assessment, the malignant lesions exhibited angled, massive and tortuous feeding arteries by rotating real-time 3D-CEUS images. Feeding artery numbers ($P = 0.005$, **Table 3**) and structures ($P = 0.017$, **Table 4**) showed significant differences between real-time 3D-CEUS and 2D-CEUS in HCC (**Figure 1**). However, no significant differences were found between 2D-CEUS and real-time 3D-CEUS in the artery numbers and structures of benign lesions ($P = 0.387$ and $P = 0.458$, respectively).

Characteristics and diagnostic performance of real-time 3D-CEUS images

We excluded 29 (29/161, 18.0%) lesions with poor image quality due to inadequate visualiza-

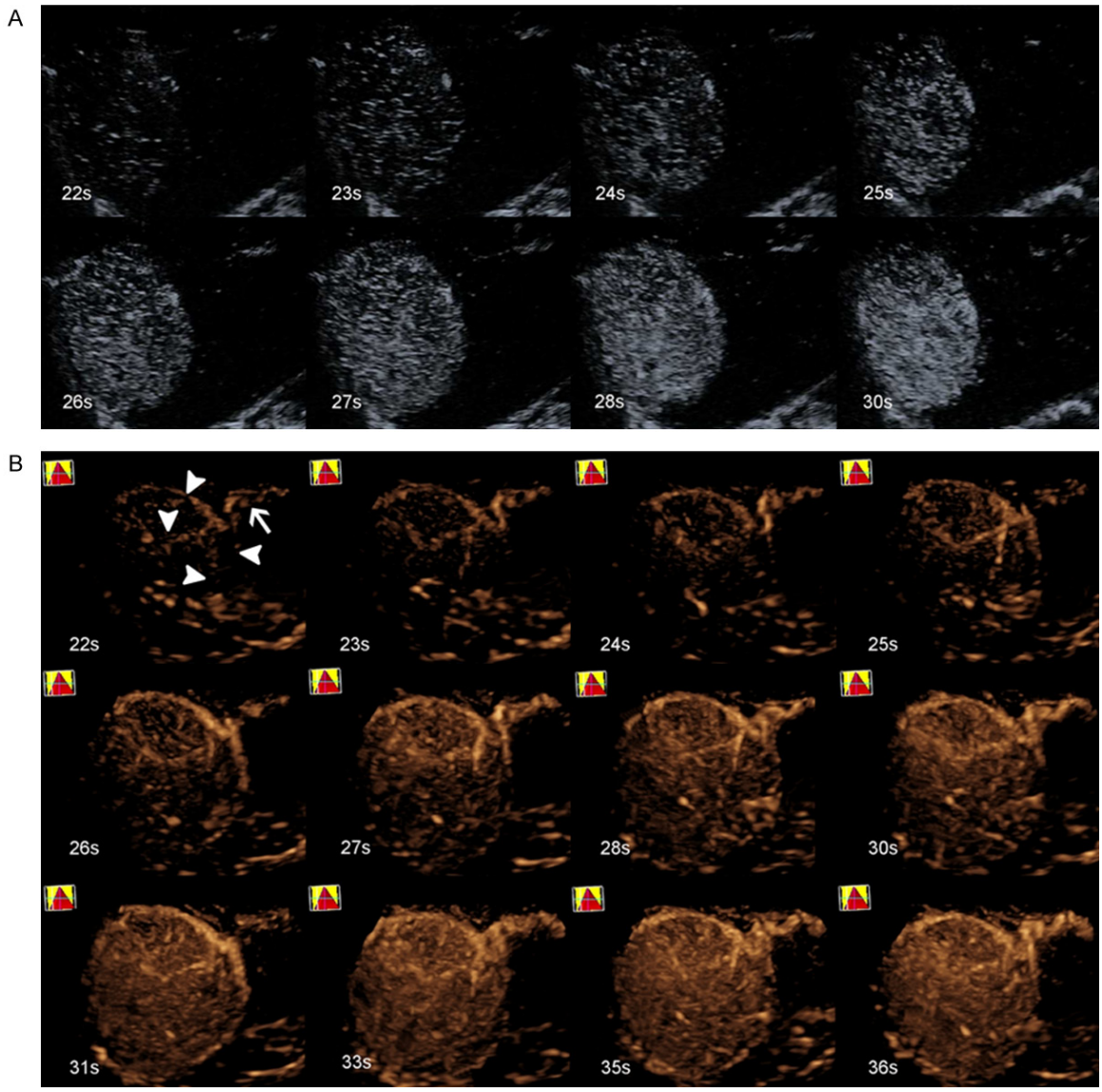

Figure 1. A 68-year-old male with HCC (tumor size, 8.1 cm × 5.6 cm) in segments V and VIII of the liver. A. 2D-CEUS did not exhibit the feeding artery during the whole process. B. Real-time 3D-CEUS showed a clear feeding artery (white arrow), with four surrounding branches (white arrowhead) supplying the lesion, which is called a surrounding pattern.

tion. Therefore, a total of 132 lesions were further analyzed for tumor vessels and tumor enhancements on the real-time 3D-CEUS images. Among them, there were 92 HCCs, 13 MLCs, 13 FNHs, and 14 hemangiomas. The tumor vessels and tumor enhancements of the 132 FLLs are presented in **Tables 5** and **6**, respectively.

HCC

Of the 92 HCCs, 87 (87/92, 94.6%) lesions had intratumoral vessels, and 48 of these had a surrounding pattern (**Figure 1**), 14 a branching pattern (**Figure 2**), and 25 a mixed artery pattern. Among them, most (86/87, 98.9%) lesions exhibited intratumoral vessels with diffuse enhancement, and only one (1/87, 1.1%) had early intratumoral vessels with rim-like enhancement. Another 5 HCC lesions exhibited rim-like enhancement: two with peritumoral vessels and three without tumor vessels. If lesions displaying intratumoral vessels with diffuse enhancement were diagnosed as HCC, the sensitivity, specificity, and accuracy were 93.5%, 85.0%, and 89.6%, respectively.

Table 5. Vascular structure of FLLs with acceptable image quality (n = 132)

		HCC (n = 92)	MLC (n = 13)	FNH (n = 13)	Hemangiomas (n = 14)
Intratumoral vessels	Surrounding	48 (53.3%)	0 (0%)	0 (0%)	0 (0%)
	Branching	14 (15.2%)	2 (15.4%)	2 (15.4%)	0 (0%)
	Mix	25 (27.2%)	2 (15.4%)	0 (0%)	0 (0%)
	Total	87 (94.6%)	4 (30.8%)	2 (15.4%)	0 (0%)
Spoke-wheel artery		0 (0%)	0 (0%)	11 (84.6%)	0 (0%)
Peritumoral vessels		2 (0%)	5 (38.5%)	0 (0%)	2 (15.3%)
Absence of tumor vessels		3 (1.1%)	5 (30.8%)	0 (0%)	12 (85.7%)

Table 6. Enhancement pattern of FLLs with acceptable image quality (n = 132)

	HCC (n = 92)	MLC (n = 13)	FNH (n = 13)	Hemangiomas (n = 14)
Diffuse enhancement	86 (93.5%)	4 (30.8%)	13 (100%)	0 (0%)
Nodular enhancement	0 (0%)	0 (0%)	0 (0%)	13 (92.9%)
Rim-like enhancement	6 (6.5%)	5 (38.4%)	0 (0%)	1 (7.1%)
Non-enhancement	0 (0%)	4 (30.8%)	0 (0%)	0 (0%)

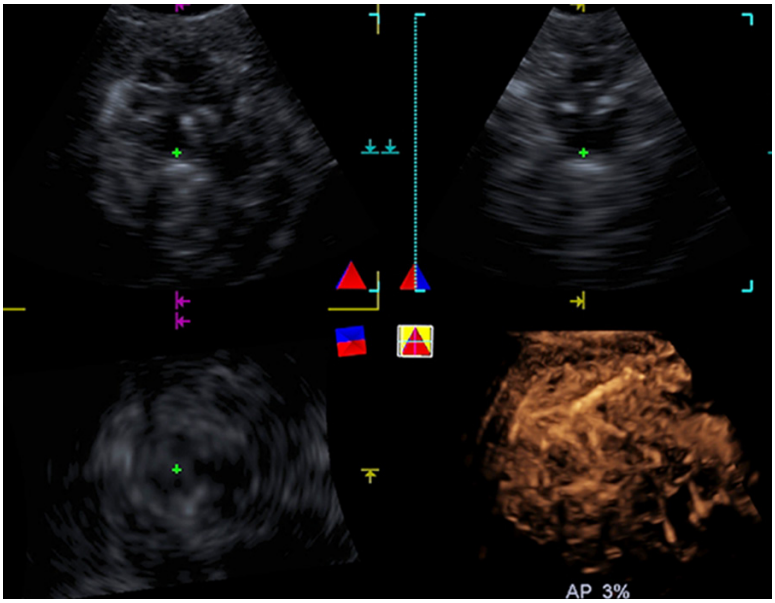

Figure 2. A 37-year-old male with HCC (tumor size, 11.7 cm × 10.7 cm) in segments V and VIII of the liver. Real-time 2D-CEUS does not exhibit the feeding artery while real-time 3D-CEUS showed diffuse enhancement with intratumoral vessels showing a branching pattern.

MLC

Different tumor vessels and tumor enhancement was detected in the 13 MLCs. Four lesions showed rim-like enhancement with peritumoral vessels (**Figure 3**), and one lesion showed rim-like enhancement without tumor vessels. Four lesions exhibited non-enhancement without tumor vessels. The remaining four lesions showed diffuse enhancement with intratumoral vessels. If lesions displaying peritumoral vessels or absence of tumor vessels with ring-like enhancement or nonenhancement were diagnosed as MLC, the sensitivity, specificity, and accuracy were 69.2%, 95.0%, and 92.4%, respectively.

FNH

There were 13 FNH lesions in the study. Eleven (11/13, 84.6%) lesions showed a spoke-wheel artery with diffuse enhancement (**Figure 4**). The remaining two (2/13, 15.4%) lesions showed intratumoral vessels with diffuse enhancement. If lesions displaying a spoke-wheel artery with diffuse enhancement were diagnosed as FNH, the sensitivity, specificity, and accuracy were 84.6%, 100%, and 98.5%, respectively.

Hemangiomas

Most (13/14, 92.9%) hemangiomas showed nodular enhancement without tumor vessels (n = 12, 92.3%) (**Figure 5**) or peritumoral vessels (n = 1, 7.7%). Only one (1/14, 7.1%) lesion had rim-like enhancement with peritumoral vessels. Lesions displaying nodular enhancement had a sensitivity of 92.9%, a specificity of

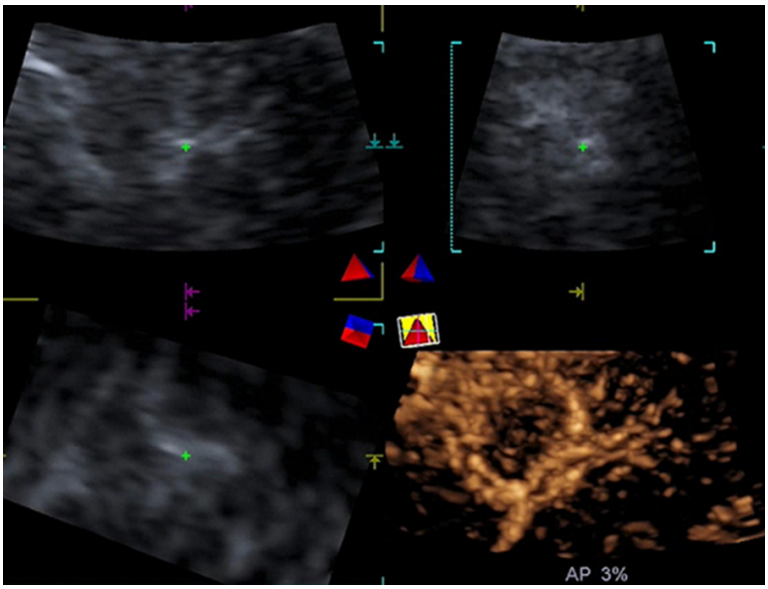

Figure 3. A 34-year-old male with MLC from rectal cancer (tumor size, 1.5 cm × 1.3 cm) in segment VI of the liver. Real-time 3D-CEUS showed rim-like enhancement with peritumoral vessels.

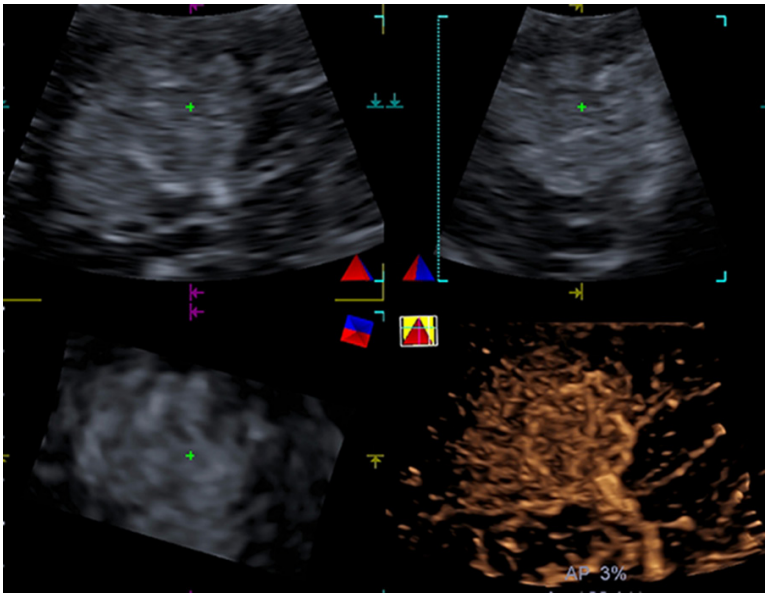

Figure 4. A 29-year-old female with FNH (tumor size, 4.7 cm × 4.4 cm) in segment V of the liver. Real-time 3D-CEUS showed a spoke-wheel artery with diffuse enhancement.

100%, and an accuracy of 99.2% for the diagnosis of hemangioma.

Discussion

In the present study, we investigated the vascular configurations of FLLs using real-time 3D-CEUS with SonoVue. Different FLLs displayed characteristic vascular structures and enhancement patterns on the real-time 3D-CEUS images, which can aid in the differential diagnosis of FLLs. Compared with 2D-CEUS, 3D-CEUS exhibited a higher spatial resolution of the continuous perfusion of the feeding vessels and their origin, distribution, and continuity. The results indicate that real-time 3D-CEUS using SonoVue is an effective method for visualizing the characteristic vascular configurations of FLLs. While the technique is effective, the scanning approach, interfering factors, and intralesional enhancement level in the arterial phase influenced the final image quality.

A growing number of studies have examined 3D-CEUS for the evaluation of FLLs [4, 10-13]. In the retrospective study of Luo et al. [14], 84 patients with FLLs underwent automatic scanning with static 3D sonography 20-60 seconds after administration of a perflubutane contrast agent. The main pattern and intratumoral vessels with early homogeneous or heterogeneous tumor enhancement had an acceptable sensitivity and specificity for FLLs. Therefore, 3D-CEUS was thought to be an alternative method for visualizing the characteristic vascularity of FLLs that may contribute to their diagnosis. Compared with 3D contrast-enhanced CT, 3D-CEUS was shown to have similar sensitivity and specificity in characterizing various FLLs [10]. However, a static 3D-CEUS technique that could not visualize dynamic perfusion was used in that study. Recently, Dong et al. [4] used dynamic 3D-CEUS to demonstrate the vascular configuration of FLLs. Nevertheless, dynamic 3D-CEUS was not real-time in that

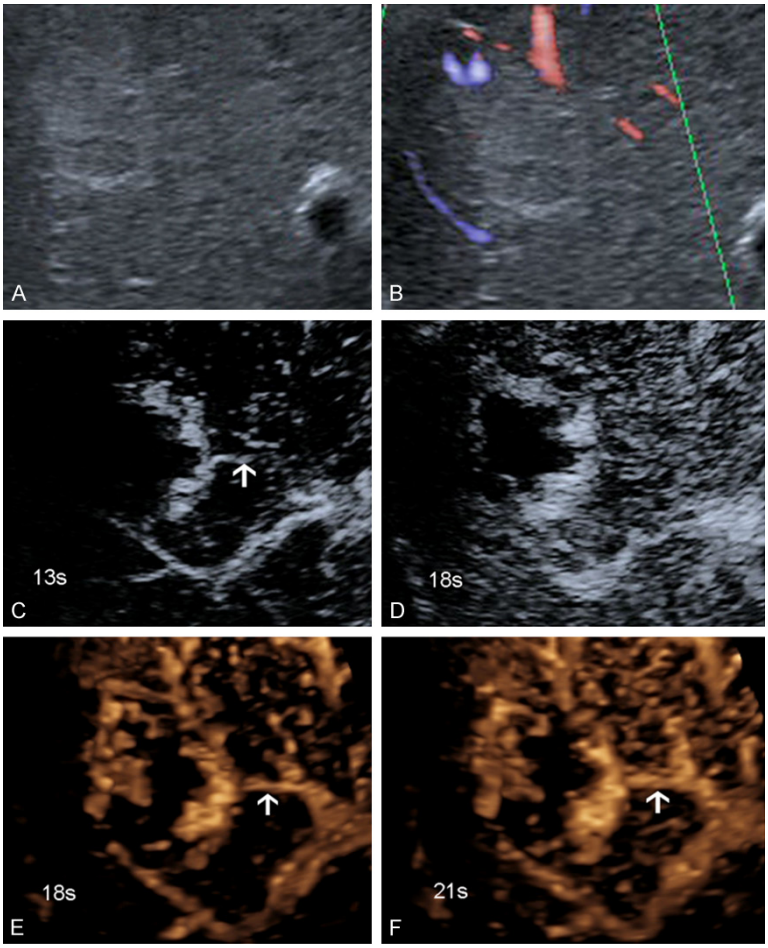

Figure 5. A 72-year-old male with hemangiomas (tumor size, 4.0 cm × 3.3 cm) in segments VII and VIII of the liver. A. US showed hypersonic lesions. B. ADFI showed no feeding artery. C, D. 2D-CEUS showed a feeding artery with an unclear origin and poor continuity. E, F. Real-time 3D-CEUS showed a clear feeding artery (white arrow), with a clear origin and good continuity.

study. A time delay is present when 3D acquisition is selected, and the 3D program is initiated [4].

In the present study, we used real-time 3D-CEUS to determine the characteristic vascularity of FLLs, and compared it with 2D-CEUS images of the feeding artery. Real-time 3D-CEUS can display the origin, continuity, and numbers and structures of the feeding arteries in the malignant lesions in more detail. No difference in terms of numbers and structures was found in benign lesions due to their small number. In fact, the feeding arteries were less tortuous in benign lesions. In some lesions, the 2D-CEUS images failed to display the feeding arteries on the initially selected sections, but the continuity and spatial relations of the arteries were clearly displayed by real-time 3D-CEUS through image post-processing. Real-time 3D-CEUS offers the advantage of providing enhanced images in the three orthogonal planes, which facilitates the review of the images from various directions and slice-by-slice in real-time. Additionally, 3D-CEUS provides detailed information about the spatial relations between the tumors and adjacent structures. Therefore, real-time 3D-CEUS may demonstrate tumor information that is missed by 2D-CEUS, and even by static 3D-CEUS. Therefore, real-time 3D-CEUS is superior to 2D-CEUS in revealing the feeding artery of FLLs.

On the real-time 3D-CEUS images, most HCCs exhibited early diffuse enhancement of intratumoral vessels, while the main enhancement patterns of hepatic hemangioma and FNHs were peripheral nodular enhancement and spoke-wheel arteries with early tumor enhancement, respectively. However, different enhancement patterns were detected in the MLCs during the arterial phase. Most MLCs displayed peritumoral vessels or absence of tumor vessels with ring-like enhancement or non-enhancement, which was consistent with the findings of Luo et al. [12]. Based upon this diagnostic criterion, the sensitivity for MLCs is relatively low. A possible explanation may be that the quick wash-out of contrast and marked hypoenhancement in the portal or late phases is the typical enhancement pattern of MLCs. However, due to the technical limitations of the current 4D probe, only the arterial phase was stored and used to differentiate FLLs in the present study.

We found that the scanning approach, interfering shadowing, and intralesional enhancement level significantly influenced the final image

quality of 3D-CEUS. In the present study, intercostal scanning was found to be beneficial in obtaining high image quality, in contrast with the results reported by Xu et al. [1]. Perhaps, most tumors scanned in the subcostal approach are likely to be influenced by heart motion or respiratory movement, which may result in signal loss during 3D scanning. On the other hand, real-time 3D-CEUS images in the arterial phase of the lesions achieved a high image quality in 92.2% of hyperenhanced, 46.2% of hypo- or non-enhanced lesions, and only 16.7% of isoenhanced lesions. Therefore, the isoenhanced lesions on CEUS are not appropriate for 3D examination because insufficient contrast is present at the interface of the lesion and surrounding liver parenchyma, as shown in unenhanced liver ultrasound scanning. Similarly, clear intralesional vascularity on 3D-CEUS was visualized in most of the hyperenhanced FLLs. Better results were obtained in hyperenhanced lesions due to a superior spatial relation, significant contrast, and the information content of the lesions.

In our department, static 3D-CEUS evaluation of the liver had been utilized for many years [15]. Recently, the 3D technique has improved, and is gradually being used in more applications, such as guidance for puncture procedures [16] and the assessment of local treatment efficacy [17, 12, 7]. In 2011, Sugimoto et al. [16] designed a liver phantom that contained four simulated spherical masses of two different sizes, and in two different positions within an acrylic box. Punctures with 2D and real-time 3D ultrasound guidance were performed and compared. The results suggested that real-time 3D ultrasound-guided punctures were markedly more accurate than 2D ultrasound-guided punctures in most tumor models of different diameters and depths. With the help of ultrasound contrast agents, the 3D technique is useful for differentiating FLLs, and also for evaluating the treatment efficacy after local therapies (such as radiofrequency ablation, microwave ablation, and transcatheter arterial chemoembolization) for malignant FLLs [17-19]. Previous studies have reported that 3D-CEUS showed highly consistent assessment of ablation efficacy for HCC compared with contrast-enhanced CT, and has the potential to serve as an alternative to contrast-enhanced CT in follow-up after ablation [18, 19]. Compared with 2D-CEUS, 3D-CEUS improved the diagnostic confidence in assessing the response of liver cancer to local therapies in the majority of patients, and even led to changes in the management of some patients [20], although the diagnostic performance is similar [20, 21].

Although real-time 3D-CEUS images were successfully reconstructed for all the FLLs, 29 FLLs including 83.3% of iso-enhanced lesions and 53.8% of hypo- or non-enhancing lesions were excluded in evaluating the diagnostic performance due to poor image quality. Moreover, we only investigated images in the arterial phase because of inadequate image quality in the portal and late phases. In spite of the improvement of the current 4D probe, the spatial resolution is still limited, especially in the portal and late phases. As such, new generation 4D probes are in development to allow uninterrupted monitoring of the 3D information.

This study has several limitations. Firstly, most lesions were malignant, and a selection bias may exist. The study population may not be representative of a screening population. Secondly, real-time 3D-CEUS images in the portal and late phases were not evaluated due to poor image quality, although these images could be obtained. Given that in 18.0% of cases, unsatisfactory 3D-CEUS image quality may impact image evaluation, these lesions were excluded in assessing the diagnostic performance. Thirdly, we used tumor enhancement patterns to differentiate FLLs, without using the characteristics of feeding arteries. Perhaps, the combination of tumor enhancement patterns and the characteristics of the feeding artery could improve the diagnostic performance of real-time 3D-CEUS; this hypothesis will be investigated in our further studies. Fourthly, the diagnostic performance of real-time 3D-CEUS in the differentiation of FLLs was not compared with 2D-CEUS. Finally, the evaluation of inter-observer agreement was not investigated; different results from the two investigators were resolved by consensus.

In conclusion, real-time 3D-CEUS using SonoVue is an effective technique for visualizing the characteristic vascular configurations of FLLs, and may contribute to the diagnosis of these lesions. Further large-scale multicenter

studies are required to confirm our observations.

Acknowledgements

National Natural Science Foundation of China (NSFC, Contract grant number: 81501493, 81530055).

Disclosure of conflict of interest

None.

Address correspondence to: Xiaoyan Xie, Department of Medical Ultrasound, Institute of Diagnostic and Interventional Ultrasound, The First Affiliated Hospital, Sun Yat-sen University, 58 Zhong Shan Road 2, Guangdong Province, P. R. China. Tel: +86-20-87765183; Fax: +86-20-87765183; E-mail: xiexy1992@126.com

References

[1] Corvino A, Catalano O, Setola SV, Sandomenico F, Corvino F, Petrillo A. Contrast-enhanced ultrasound in the characterization of complex cystic focal liver lesions. Ultrasound Med Biol 2015; 41: 1301-1310.

[2] Piscaglia F, Lencioni R, Sagrini E, Pina CD, Cioni D, Vidili G, Bolondi L. Characterization of focal liver lesions with contrast-enhanced ultrasound. Ultrasound Med Biol 2010; 36: 531-550.

[3] Strobel D, Seitz K, Blank W, Schuler A, Dietrich CF, von Herbay A, Friedrich-Rust M, Bernatik T. Tumor-specific vascularization pattern of liver metastasis, hepatocellular carcinoma, hemangioma and focal nodular hyperplasia in the differential diagnosis of 1,349 liver lesions in contrast-enhanced ultrasound (CEUS). Ultraschall Med 2009; 30: 376-382.

[4] Dong FJ, Xu JF, Du D, Jiao Y, Zhang L, Li M, Liu HY, Xiong Y, Luo H. 3D analysis is superior to 2D analysis for contrast-enhanced ultrasound in revealing vascularity in focal liver lesions-A retrospective analysis of 83 cases. Ultrasonics 2016; 70: 221-226.

[5] Li QY, Tang J, He EH, Li YM, Zhou Y, Zhang X, Chen G. Clinical utility of three-dimensional contrast-enhanced ultrasound in the differentiation between noninvasive and invasive neoplasms of urinary bladder. Eur J Radiol 2012; 81: 2936-2942.

[6] Luo W, Numata K, Morimoto M, Nozaki A, Nagano Y, Sugimori K, Tanaka K. Three-dimensional contrast-enhanced sonography of vascular patterns of focal liver tumors: pilot study of visualization methods. AJR Am J Roentgenol 2009; 192: 165-173.

[7] Wang Z, Wang W, Liu GJ, Yang Z, Chen LD, Huang Y, Li W, Xie XY, Lu MD, Kuang M. The role of quantitation of real-time 3-dimensional contrast-enhanced ultrasound in detecting microvascular invasion: an in vivo study. Abdom Radiol (NY) 2016; 41: 1973-199.

[8] Sporea I, Badea R, Popescu A, Sparchez Z, Sirli RL, Danila M, Sandulescu L, Bota S, Calescu DP, Nedelcu D, Brisc C, Ciobaca L, Gheorghe L, Socaciu M, Martie A, Ioanitescu S, Tamas A, Streba CT, Iordache M, Simionov I, Jinga M, Anghel A, Cijevschi Prelipcean C, Mihai C, Stanciu SM, Stoicescu D, Dumitru E, Pietrareanu C, Bartos D, Manzat Saplacan R, Parvulescu I, Vadan R, Smira G, Tuta L, Saftoiu A. Contrast-enhanced ultrasound (CEUS) for the evaluation of focal liver lesions-a prospective multicenter study of its usefulness in clinical practice. Ultraschall Med 2014; 35: 259-266.

[9] Claudon M, Dietrich CF, Choi BI, Cosgrove DO, Kudo M, Nolsoe CP, Piscaglia F, Wilson SR, Barr RG, Chammas MC, Chaubal NG, Chen MH, Clevert DA, Correas JM, Ding H, Forsberg F, Fowlkes JB, Gibson RN, Goldberg BB, Lassau N, Leen EL, Mattrey RF, Moriyasu F, Solbiati L, Weskott HP, Xu HX; World Federation for Ultrasound in Medicine; European Federation of Societies for Ultrasound. Guidelines and good clinical practice recommendations for Contrast enhanced ultrasound (CEUS) in the liver-update 2012: A WFUMB-EFSUMB initiative in cooperation with representatives of AFSUMB, AIUM, ASUM, FLAUS and ICUS. Ultrasound Med Biol 2013; 39: 187-210.

[10] Luo W, Numata K, Morimoto M, Kondo M, Takebayashi S, Okada M, Morita S, Tanaka K. Focal liver tumors: characterization with 3D perflubutane microbubble contrast agent-enhanced US versus 3D contrast-enhanced multidetector CT. Radiology 2009; 251: 287-295.

[11] Luo W, Numata K, Morimoto M, Nozaki A, Nagano Y, Sugimori K, Zhou X, Tanaka K. Clinical utility of contrast-enhanced three-dimensional ultrasound imaging with Sonazoid: findings on hepatocellular carcinoma lesions. Eur J Radiol 2009; 72: 425-431.

[12] Luo W, Numata K, Morimoto M, Nozaki A, Ueda M, Kondo M, Morita S, Tanaka K. Differentiation of focal liver lesions using three-dimensional ultrasonography: retrospective and prospective studies. World J Gastroentero 2010; 16: 2109-2119.

[13] Ohto M, Kato H, Tsujii H, Maruyama H, Matsutani S, Yamagata H. Vascular flow patterns of hepatic tumors in contrast-enhanced 3-dimensional fusion ultrasonography using plane shift and opacity control modes. J Ultrasound Med 2005; 24: 49-57.

[14] Luo W, Numata K, Morimoto M, Nozaki A, Nagano Y, Sugimori K, Tanaka K. Three-dimensional contrast-enhanced sonography of vascular patterns of focal liver tumors: pilot study of visualization methods. AJR Am J Roentgenol 2009; 192: 165-173.

[15] Xu HX, Lu MD, Xie XH, Xie XY, Xu ZF, Chen LD, Liu GJ, Liang JY, Lin MX, Wang Z, Huang B. Three-dimensional contrast-enhanced ultrasound of the liver: experience of 92 cases. Ultrasonics 2009; 49: 377-385.

[16] Sugimoto K, Moriyasu F, Shiraishi J, Yamada M, Imai Y. A phantom study comparing ultrasound-guided liver tumor puncture using new real-time 3D ultrasound and conventional 2D ultrasound. AJR Am J Roentgenol 2011; 196: W753-757.

[17] Fleckenstein FN, Schernthaner RE, Duran R, Sohn JH, Sahu S, Marshall K, Lin M, Gebauer B, Chapiro J, Salem R, Geschwind JF. Renal cell carcinoma metastatic to the liver: early response assessment after intraarterial therapy using 3d quantitative tumor enhancement analysis. Transl Oncol 2016; 9: 377-83.

[18] Luo W, Numata K, Morimoto M, Oshima T, Ueda M, Okada M, Takebayashi S, Zhou X, Tanaka K. Role of Sonazoid-enhanced three-dimensional ultrasonography in the evaluation of percutaneous radiofrequency ablation of hepatocellular carcinoma. Eur J Radiol 2010; 75: 91-97.

[19] Wang Y, Jing X, Ding J. Clinical value of dynamic 3-dimensional contrast-enhanced ultrasound imaging for the assessment of hepatocellular carcinoma ablation. Clin Imaging 2016; 40: 402-406.

[20] Xu HX, Lu MD, Xie XH, Xie XY, Kuang M, Xu ZF, Liu GJ, Wang Z, Chen LD, Lin MX. Treatment response evaluation with three-dimensional contrast-enhanced ultrasound for liver cancer after local therapies. Eur J Radiol 2010; 76: 81-88.

[21] Bartolotta TV, Taibbi A, Matranga D, Midiri M, Lagalla R. 3D versus 2D contrast-enhanced sonography in the evaluation of therapeutic response of hepatocellular carcinoma after locoregional therapies: preliminary findings. Radiol Med 2015; 120: 695-704.